IEEE Access
Multidisciplinary | Rapid Review | Open Access Journal

Received 19 May 2024, accepted 5 June 2024, date of publication 11 June 2024, date of current version 20 June 2024.

Digital Object Identifier 10.1109/ACCESS.2024.3412819

RESEARCH ARTICLE

Stability Criterion of DC-DC Converter With Different Loads Based on Mixed Potential Theory

YUFEI LI, (Graduate Student Member, IEEE), FEI WANG, (Senior Member, IEEE), YUXIN ZHU, (Student Member, IEEE), AND HUI GUO, (Member, IEEE)
School of Mechatronic Engineering and Automation, Shanghai University, Shanghai 200444, China
Corresponding author: Fei Wang (f.wang@i.shu.edu.cn)

This work was supported by the National Natural Science Foundation of China under Grant 51977126.

ABSTRACT The dc systems consisting of power electronic converters always suffer from various stability problems, and the mixed potential theory (MPT) has been widely applied to study these problems in recent years because the stability criterion in analytical form can be derived easily. However, the models of the dc-dc converters in most studies are simplified, and thus only the control parameters at system level are considered. Some work has done to propose the MPT criterion based on complete converter models which involve the control parameters of the converters but such improved MPT criterion is optimistic for system stability. This paper proposes the MPT criterion of a boost converter with different loads based on complete converter models and expounds the mathematical features and the physical implication of the proposed MPT criterion. The proposed MPT criterion can be used for the design of system parameters but it is a necessary condition for system stability. The reasons for the optimism of the proposed criterion are revealed from the expounded mathematical features and physical implication. Finally, real-time simulations are conducted in RT-LAB to verify the correctness of the theoretical analyses.

INDEX TERMS Stability criterion, mixed potential theory, mathematical feature, physical implication.

NOMENCLATURE

$P(\boldsymbol{i}, \boldsymbol{u})$	Mixed potential function.
$\boldsymbol{i}^*$	Set of inductor currents.
$\boldsymbol{u}^*$	Set of capacitor voltages.
μ	Index of resistor branches and source branches.
σ	Index of capacitor branches.
ρ	Index of inductor branches.
$A(\boldsymbol{i})$	Current potential.
$B(\boldsymbol{u})$	Voltage potential.
$(\boldsymbol{i}, \gamma\boldsymbol{u}\text{-}\alpha)$	Mixed potential.
γ	Matrix of structure parameters.
α	Matrix of sources.
μ_1, μ_2	Smallest eigenvalues of matrices.
$\lambda_{\min}$	Index of smallest eigenvalues.
$\boldsymbol{A}_{\mathrm{ii}}(\boldsymbol{i})$	Second-order partial derivate matrix of $A(\boldsymbol{i})$.
$\boldsymbol{B}_{\mathrm{uu}}(\boldsymbol{u})$	Second-order partial derivate matrix of $B(\boldsymbol{u})$.
$\boldsymbol{P}_{\mathrm{i}}$	Partial derivate matrix of $A(\boldsymbol{i})$.
$\boldsymbol{P}_{\mathrm{u}}$	Partial derivate matrix of $B(\boldsymbol{u})$.
u_{o}	Output voltage of converter.
i_L	Input current of converter.
u_{oref}	Reference of output voltage u_{o}.
$i_{L\mathrm{ref}}$	Reference of input current i_L.
u_{in}	Source voltage of converter.
i_{o}	Output current of converter.
u_{c}	Modulation signal in dual closed-loop control.
d	Duty ratio in dual closed-loop control.
G_{cu}	PI controller of voltage loop.
G_{ci}	PI controller of current loop.
k_{pu}	proportional coefficient of G_{cu}.
k_{iu}	Integral coefficient of G_{cu}.
k_{pi}	Proportional coefficient of G_{ci}.
k_{ii}	Integral coefficient of G_{ci}.

The associate editor coordinating the review of this manuscript and approving it for publication was Zhe Zhang.

R_{MPT}	Load limit of R given by MPT.
i_{MPT}	Load limit of i_{Load} given by MPT.
P_{MPT}	Load limit of P_{Load} given by MPT.
G_{id}	Transfer function from $\hat{d}$ to $\hat{i}_L$.
G_{ui}	Transfer function from $\hat{i}_L$ to $\hat{u}_{\mathrm{o}}$.
G_{i}	Transfer function of current loop.
G_{u}	Transfer function of closed loop.
G_i^*	Simplified transfer function of current loop.
G_u^*	Simplified transfer function of closed loop.
τ	Time constant related to bandwidth.
f_{s}	Switching frequency.
R_{Hurwitz}	Load limit of R given by Hurwitz criterion.
i_{Hurwitz}	Load limit of i_{Load} given by Hurwitz criterion.
P_{Hurwitz}	Load limit of P_{Load} given by Hurwitz criterion.
U_{co}	Initial voltage of capacitor.
R_{Surface}	Load limit of R given by geometric method.
i_{Surface}	Load limit of i_{Load} given by geometric method.
P_{Surface}	Load limit of P_{Load} given by geometric method.
$R_{\mathrm{RT-LAB}}$	Load limit of R given by RT-LAB.
$i_{\mathrm{RT-LAB}}$	Load limit of i_{Load} given by RT-LAB.
$P_{\mathrm{RT-LAB}}$	Load limit of P_{Load} given by RT-LAB.

I. INTRODUCTION

As the medium transmitting power between dc units, dc-dc converter has great impacts on the stability of the dc system containing distributed generations, storage devices and dc loads [1], [2]. Specifically, the system consisting of dc-dc converters is always facing unstable inducements [3], [4], such as the disturbances of loads [5], [6], the oscillations caused by the impedance mismatch between different converters [7], [8] and the reduction of the system damping brought by constant power loads [9], [10]. In order to study the stability of the dc systems consisting of dc-dc converters, large-signal analysis methods based on Lyapunov functions have been gradually applied in recent years [11], [12].

The Takagi-Sugeno model method (T-S), the block-diagonalized quadratic Lyapunov function method (BDQLF) and the reverse trajectory tracking method are usually used to establish Lyapunov functions [13], [14] but only qualitative stability criteria can be derived. The Hamiltonian surface shaping method [15], [16], the potential energy boundary surface (PEBS) method [17], [18] and the methods based on the passivity theory [19], [20] can give stability criteria in analytical form, while they are subject to the scale of the systems and the obtained stability domains are conservative. Comparatively, the mixed potential theory (MPT) is more suitable for the stability analysis and the parameter design of dc systems because the Lyapunov energy functions can be established easily and the stability criteria in analytical form can be derived directly [21], [22]. For instance, the influences of system parameters on the stability of a droop-controlled dc microgrid are studied in [23] based on the MPT. Similar work is conducted on a VSC-HVDC system in [24], and the boundaries of control parameters are generated from the MPT criterion. For a hybrid multi-terminal HVDC system in [25], the optimal control parameters are obtained from a dynamic performance evaluation function established based on the MPT criterion. In addition, specific control schemes can be developed by combining the MPT and other methods, such as the decentralized voltage control proposed in [26] which is robust to the unknown ZIP loads in dc power networks.

Although it is easy and convenient to use the MPT, there is a consensus among most studies that the stability domains obtained by the traditional MPT are still conservative [21], [22], [23], [24], [25], [26], [27]. As a consequence, a revised MPT criterion which is the sufficient condition for the stability of dc power girds is proposed in [27] and applied in [28] to obtain more accurate stability domain. Further, a hyperlocal large-signal stability analysis method is proposed in [29] based on such revised MPT for large-scale complex power grids. However, only the influence of control parameters at system level on system stability can be studied by the traditional MPT or the revised MPT because dc-dc converters are usually treated as voltage or current sources during system modeling [21], [22], [23], [24], [25], [26], [27], [28], [29]. By contrast, the improved MPT criteria proposed in [30], [31], and [32] consider the complete models of dc-dc converters and thus involve all the control parameters. While the stability domains obtained in [30], [31], and [32] show optimism instead of conservatism, which indicates that such improved MPT criterion considering the control parameters is actually the necessary condition for system stability. Therefore, there is a great need to investigate the characteristics of the MPT criterion which is proposed based on complete converter models, and find the reason for the optimism of such MPT criterion which involves both the circuit parameters and the control parameters of the system.

To address the issues, this paper starts with the stability analysis of a boost-converter system based on the MPT. For convenience of analysis, the boost converter is considered operating in continuous current mode (CCM) because there are fewer nonlinearities in the circuit. The small-signal model of the boost converter is established and used as the complete converter model. The MPT criterion is proposed in different load cases respectively which involve constant impedance load (CIL), constant current load (CCL) and constant power load (CPL). The characteristics of the proposed MPT criterion include mathematical features and physical implication. The mathematical features are revealed by comparing with the Hurwitz criterion which is a sufficient and necessary condition for system stability. The physical implication is interpreted from the aspect of control principle to reveal the reason for the optimism of the proposed MPT criterion. Additionally, the necessity of the proposed MPT criterion for system stability is identified based on these characteristics. The verifications of the optimism and the effectiveness of the proposed MPT criterion are conducted based on real-time simulations instead of experiments.

This paper is organized as follows. Section II introduces the mixed potential theory and proposes the MPT

criterion in CIL/CCL/CPL case. In Section III, the characteristics of the proposed MPT criterion are expounded which include the mathematical features and the physical implication. The results of the real-time simulations are provided in Section IV. The conclusions are drawn in Section V.

II. STABILITY ANALYSIS BASED ON MPT

The mixed potential theory was first proposed in 1964 for the stability analysis of nonlinear circuits [21]. Therefore, the system consisting of dc-dc converters can be analyzed by the MPT to obtain stability criterion.

A. INTRODUCTION OF THE MIXED POTENTIAL THEORY

For a "complete" circuit defined in [21], the mixed potential function P can be established as (1) which contains mixed terms of voltage multiplied by current.

$$P(\boldsymbol{i}^*, \boldsymbol{u}^*) = \int_{\Gamma} \sum_{\mu > \mathrm{r+s}} u_\mu di_\mu + \sum_{\sigma=\mathrm{r}+1}^{\mathrm{r+s}} i_\sigma u_\sigma \Bigg|_{\Gamma} \tag{1}$$

where $\boldsymbol{i}^* = (i_1, \ldots, i_\mathrm{r})$ and $\boldsymbol{u}^* = (u_{\mathrm{r}+1}, \ldots, u_{\mathrm{r+s}})$ respectively represent the set of inductor currents and capacitor voltages in the circuit. The integral part is the total current potential of the elements in the branches labeled as μ, except inductors and capacitors. The second part denotes the sum of each capacitor current multiplied by capacitor voltage.

In addition, the function P can also be derived from and verified by the differential equations of the circuit. The corresponding formulars are presented as

$$\begin{cases} L_\rho \dfrac{di_\rho}{dt} = \dfrac{\partial P}{\partial i_\rho}, & (\rho = 1, \ldots, \mathrm{r}) \\ C_\sigma \dfrac{du_\sigma}{dt} = -\dfrac{\partial P}{\partial u_\sigma}, & (\sigma = \mathrm{r}+1, \ldots, \mathrm{r+s}) \end{cases} \tag{2}$$

where L_ρ ($\rho = 1, \ldots, \mathrm{r}$) are the inductors in the circuit and C_σ ($\sigma = \mathrm{r}+1, \ldots, \mathrm{r+s}$) are the capacitors.

The construction approach to the function is presented in [21], and the function can be written in a standard form as

$$P(\boldsymbol{i}, \boldsymbol{u}) = -A(\boldsymbol{i}) + B(\boldsymbol{u}) + (\boldsymbol{i}, \boldsymbol{\gamma u} - \boldsymbol{a}) \tag{3}$$

It can be seen that the function consists of three parts: the current potential -$A(\boldsymbol{i})$, the voltage potential $B(\boldsymbol{u})$, and a mixed term related to a constant matrix γ decided by the structure of the circuit and a constant vector $\boldsymbol{a}$ decided by the sources in the circuit.

According to [21], the stability criterion of the circuit can be derived from the function P that if for all i and u,

$$\begin{aligned} \mu_1 + \mu_2 = {} & \lambda_{\min}\{\boldsymbol{L}^{-1/2}\boldsymbol{A}_{\mathrm{ii}}(\boldsymbol{i})\boldsymbol{L}^{-1/2}\} \\ & + \lambda_{\min}\{\boldsymbol{C}^{-1/2}\boldsymbol{B}_{\mathrm{uu}}(\boldsymbol{u})\boldsymbol{C}^{-1/2}\} \geq \delta, \delta > 0 \end{aligned} \tag{4}$$

and

$$\begin{aligned} P^*(\boldsymbol{i}, \boldsymbol{u}) = {} & \left(\frac{\mu_1 - \mu_2}{2}\right) P(\boldsymbol{i}, \boldsymbol{u}) \\ & + \frac{1}{2}(\boldsymbol{P}_\mathrm{i}, \boldsymbol{L}^{-1}\boldsymbol{P}_\mathrm{i}) + \frac{1}{2}(\boldsymbol{P}_\mathrm{u}, \boldsymbol{C}^{-1}\boldsymbol{P}_\mathrm{u}) \end{aligned} \tag{5}$$

$$P^*(\boldsymbol{i}, \boldsymbol{u}) \to \infty \mathrm{as} |\boldsymbol{i}| + |\boldsymbol{u}| \to \infty \tag{6}$$

then all solutions of (2) approach the equilibrium solutions when $t \to \infty$.

The symbols above are defined as follows:

a. $\boldsymbol{L}$ and $\boldsymbol{C}$ respectively represent the inductor matrix and the capacitor matrix.

b. $\boldsymbol{P}_\mathrm{i}$ and $\boldsymbol{P}_\mathrm{u}$ are the partial derivative matrices of P, where $\boldsymbol{P}_\mathrm{i} = \partial P(\boldsymbol{i}, \boldsymbol{u})/\partial \boldsymbol{i}$ and $\boldsymbol{P}_\mathrm{u} = \partial P(\boldsymbol{i}, \boldsymbol{u})/\partial \boldsymbol{u}$.

c. $\boldsymbol{A}_{\mathrm{ii}}(\boldsymbol{i})$ and $\boldsymbol{B}_{\mathrm{uu}}(\boldsymbol{u})$ are the second-order partial derivative matrices of $A(\boldsymbol{i})$ and $B(\boldsymbol{u})$, where $\boldsymbol{A}_{\mathrm{ii}}(\boldsymbol{i}) = \partial^2 A(\boldsymbol{i})/\partial i^2$ and $\boldsymbol{B}_{\mathrm{uu}}(\boldsymbol{u}) = \partial^2 B(\boldsymbol{u})/\partial u^2$.

d. μ_1 and μ_2 are defined as the smallest eigenvalues of the matrices, and $\lambda_{\min}\{\cdot\}$ denotes the operator notation.

B. STABILITY CRITERIA AND LOAD LIMITS OBTAINED BY MPT

The system studied in this paper is shown in Fig.1. The boost converter adopts the voltage-current dual closed-loop control to maintain the output voltage, where u_{oref} and $i_{L\mathrm{ref}}$ are respectively the references of the output voltage u_o and the input current i_L. The PI controllers of the dual loop are marked as G_{cu} and G_{ci}, where k_{pu} and k_{iu} are the proportional coefficient and the integral coefficient of G_{cu}, and k_{pi} and k_{ii} are those of G_{ci}. The modulation signal u_c decided by G_{cu} is sent to the PWM modulator, and the duty ratio d generated are used to control the switch S. u_{in} is the source voltage and i_o is the output current. Different loads are connected to the converter for case discussions, such as CIL, CCL and CPL.

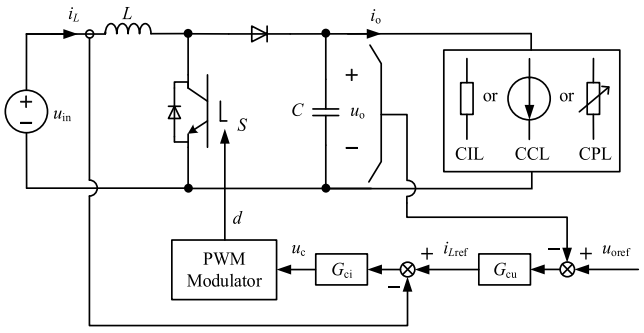

FIGURE 1. Diagram of circuit structure and control scheme.

The state space averaging equations of the system are presented as

$$\begin{cases} L\dfrac{di_L}{dt} = u_{\mathrm{in}} - (1-d)u_\mathrm{o} \\ C\dfrac{du_\mathrm{o}}{dt} = (1-d)i_\mathrm{L} - i_\mathrm{o} \end{cases} \tag{7}$$

It is noteworthy that the complex terms $(1-d)u_\mathrm{o}$ and $(1-d)i_\mathrm{L}$ in (7) make the circuit neither passive nor complete [21]. Therefore, the complex terms should be linearized to obtain the small-signal model which is regarded as the complete model of the system.

The small-signal model in CIL case is presented as (8) and the equivalent circuit is shown in Fig.2, where a constant

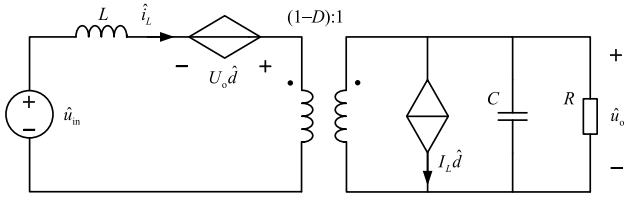

FIGURE 2. Equivalent circuit of the system in CIL case.

resistor R is used as CIL.

$$\begin{cases} L\dfrac{d\hat{i}_L}{dt} = \hat{u}_{in} + U_o\hat{d} - (1-D)\hat{u}_o \\ C\dfrac{d\hat{u}_o}{dt} = (1-D)\hat{i}_L - I_L\hat{d} - \dfrac{\hat{u}_o}{R} \end{cases} \tag{8}$$

According to Section A, the mixed potential function P can be established as

$$P(\hat{i}_L, \hat{u}_o) = \int_0^{\hat{i}_L} (U_o\hat{d})di + \int_0^{\hat{u}_o} (I_L\hat{d})du + \frac{1}{2}\frac{\hat{u}_o^2}{R} - (1-D)\hat{i}_L\hat{u}_o + \hat{i}_L\hat{u}_{in} \tag{9}$$

where the first curvilinear integral is the current potential, the voltage potential consists of the second curvilinear integral and the square term, and the remains are the mixed potential.

Considering the dual closed-loop control, the duty ratio is expressed as

$$\hat{d} = k_{pi}\left[k_{pu}(\hat{u}_{oref} - \hat{u}_o) + k_{iu}\int(\hat{u}_{oref} - \hat{u}_o)dt - \hat{i}_L\right] + k_{ii}\int\left[k_{pu}(\hat{u}_{oref} - \hat{u}_o) + k_{iu}\int(\hat{u}_{oref} - \hat{u}_o)dt - \hat{i}_L\right]dt \tag{10}$$

Based on (4) and (10), the stability criterion in CIL case can be derived from (9) as

$$\mu_1 + \mu_2 = \frac{U_o}{L}k_{pi} - \frac{I_L}{C}k_{pu}k_{pi} + \frac{1}{CR} > 0 \tag{11}$$

Meanwhile, the extended function P^* is expressed as

$$P^*(\hat{i}_L, \hat{u}_o) = \left(\frac{U_o}{2L}k_{pi} + \frac{I_L}{2C}k_{pu}k_{pi} - \frac{1}{2CR}\right)P(\hat{i}_L, \hat{u}_o) + \frac{(\hat{u}_{in} + U_o\hat{d} - (1-D)\hat{u}_o)^2}{2L} + \frac{(I_L\hat{d} + \hat{u}_o/R - (1-D)\hat{i}_L)^2}{2C} \tag{12}$$

It is obvious that $P^* \to \infty$ when $|\hat{i}_L| + |\hat{u}_o| \to \infty$, and thus the system can reach the equilibrium solutions of (8) when $t \to \infty$.

The expression (11) indicates that the system stability is related to converter parameters L, C, control parameters k_{pu}, k_{pi}, output voltage U_o, input current I_L and load R. In practical systems, L and C are usually unchanged, and thus the system stability can be guaranteed by the proper design of k_{pu}, k_{pi}.

In addition, the system stability is also influenced by the load when the system parameters and the output voltage are fixed. For instance, it can be found from (11) that the smaller the value of R is, the larger the sum of μ_1 and μ_2 is, and finally the more stable the system is. Therefore, the stability domain of the load is necessary to be obtained and is regarded as an index to illustrate the optimism of the proposed MPT criterion in the following analyses.

Taking into account power balance equation, the stability domain of R can be derived as (13), where the load limit of R is defined as R_{MPT}.

$$R > R_{MPT} = \frac{L\left(k_{pu}k_{pi}U_o^2 - U_{in}\right)}{k_{pi}U_{in}U_oC} \tag{13}$$

In CCL case, a constant current source i_{Load} is used as CCL, and the equivalent circuit is shown in Fig.3. The small-signal model is presented as (14), and the stability criterion can be derived as (15).

$$\begin{cases} L\dfrac{d\hat{i}_L}{dt} = \hat{u}_{in} + U_o\hat{d} - (1-D)\hat{u}_o \\ C\dfrac{d\hat{u}_o}{dt} = (1-D)\hat{i}_L - I_L\hat{d} - i_{Load} \end{cases} \tag{14}$$

$$\mu_1 + \mu_2 = \frac{U_o}{L}k_{pi} - \frac{I_L}{C}k_{pu}k_{pi} > 0 \tag{15}$$

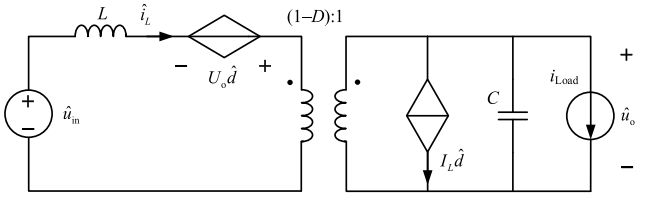

FIGURE 3. Equivalent circuit of the system in CCL case.

The extended function P^* is presented as (16) and satisfies the condition that $P^* \to \infty$ when $|\hat{i}_L| + |\hat{u}_o| \to \infty$. Hence, based on (15), the system can reach the equilibrium solutions.

$$P^*(\hat{i}_L, \hat{u}_o) = \left(\frac{U_o}{2L}k_{pi} + \frac{I_L}{2C}k_{pu}k_{pi}\right)P(\hat{i}_L, \hat{u}_o) + \frac{(\hat{u}_{in} + U_o\hat{d} - (1-D)\hat{u}_o)^2}{2L} + \frac{(I_L\hat{d} + i_{Load} - (1-D)\hat{i}_L)^2}{2C} \tag{16}$$

The stability domain of i_{Load} can be derived from (15) as (17), and i_{MPT} represents the load limit of i_{Load}.

$$i_{Load} < i_{MPT} = \frac{U_{in}C}{k_{pu}L} \tag{17}$$

In [22], [23], [24], [25], [26], [27], [28], [29], [30], and [31], CPL usually refers to tight regulated power electronic load. For universality, a nonlinear resistor P_{Load} set to constant power is regarded as CPL in this paper. The equivalent

circuit is shown in Fig.4.

$$\begin{cases} L\dfrac{d\hat{i}_L}{dt} = \hat{u}_{\text{in}} + U_{\text{o}}\hat{d} - (1-D)\hat{u}_{\text{o}} \\ C\dfrac{d\hat{u}_{\text{o}}}{dt} = (1-D)\hat{i}_L - I_L\hat{d} + \dfrac{P_{\text{Load}}}{U_{\text{o}}^2}\hat{u}_{\text{o}} \end{cases} \tag{18}$$

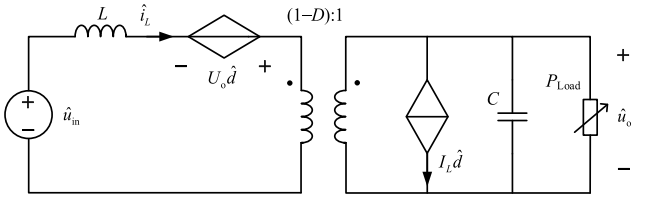

FIGURE 4. Equivalent circuit of the system in CPL case.

Then, the stability criterion can be derived as (19) from the small-signal model presented as (18).

$$\mu_1 + \mu_2 = \frac{U_{\text{o}}}{L}k_{\text{pi}} - \frac{I_L}{C}k_{\text{pu}}k_{\text{pi}} - \frac{1}{C}\frac{P_{\text{Load}}}{U_{\text{o}}^2} > 0 \tag{19}$$

The extended function P^* is presented as (20) and satisfies the condition that $P^* \to \infty$ when $|\hat{i}_L| + |\hat{u}_{\text{o}}| \to \infty$. Hence, based on (19), the system can reach the equilibrium solutions.

$$\begin{aligned} P^*(\hat{i}_L, \hat{u}_{\text{o}}) = &\left(\frac{U_{\text{o}}}{2L}k_{\text{pi}} + \frac{I_L}{2C}k_{\text{pu}}k_{\text{pi}} + \frac{1}{2C}\frac{P_{\text{Load}}}{U_{\text{o}}^2}\right)P(\hat{i}_L, \hat{u}_{\text{o}}) \\ &+ \frac{(\hat{u}_{\text{in}} + U_{\text{o}}\hat{d} - (1-D)\hat{u}_{\text{o}})^2}{2L} \\ &+ \frac{(I_L\hat{d} - P_{\text{Load}}\hat{u}_{\text{o}}/U_{\text{o}}^2 - (1-D)\hat{i}_L)^2}{2C} \end{aligned} \tag{20}$$

The stability domain of P_{Load} can be obtained as (21) from (19), and P_{MPT} represents the load limit of P_{Load}.

$$P_{\text{Load}} < P_{\text{MPT}} = \frac{k_{\text{pi}}U_{\text{in}}U_{\text{o}}^3C}{L(k_{\text{pu}}k_{\text{pi}}U_{\text{o}}^2 + U_{\text{in}})} \tag{21}$$

III. MATHEMATICAL FEATURES AND PHYSICAL IMPLICATION

The mathematical features of the MPT criterion proposed in Section II are revealed in this section by comparing with the Hurwitz criterion, and the physical implication of the features is interpreted by the geometric method from the aspect of control principle.

A. MATHEMATICAL RELATIONSHIP BETWEEN TWO CRITERIA

As another kind of stability criterion derived from small-signal model, the Hurwitz criterion is actually subject to system scales because high-order characteristic equations are difficult to be solved [33], [34], [35], [36]. In order to obtain the Hurwitz criterion for comparison, the system in this paper needs to be simplified.

Take the CIL case for example, the transfer functions of the circuit part in Fig.1 are expressed as (22) and (23). G_{id} and G_{ui} respectively represent the links from $\hat{d}$ to $\hat{i}_L$ and from $\hat{i}_L$ to $\hat{u}_{\text{o}}$.

$$G_{\text{id}} = \left.\frac{\hat{i}_L}{\hat{d}}\right|_{\hat{u}_{\text{in}}=0} = \frac{U_{\text{o}}Cs + I_L(1-D) + \frac{U_{\text{o}}}{R}}{LCs^2 + \frac{L}{R}s + (1-D)^2} \tag{22}$$

$$G_{\text{ui}} = \left.\frac{\hat{u}_{\text{o}}}{\hat{i}_L}\right|_{\hat{u}_{\text{in}}=0} = \frac{-I_LLs + (1-D)U_{\text{o}}}{U_{\text{o}}Cs + I_L(1-D) + \frac{U_{\text{o}}}{R}} \tag{23}$$

The transfer function of the current loop is defined as

$$G_{\text{i}} = \frac{\hat{i}_L}{\hat{i}_{L\text{ref}}} = \frac{G_{\text{ci}}G_{\text{id}}}{1 + G_{\text{ci}}G_{\text{id}}} = \frac{b_0s^2 + b_1s + b_2}{a_0s^3 + a_1s^2 + a_2s + a_3} \tag{24}$$

where $a_0 = LC$, $a_1 = k_{\text{pi}}U_{\text{o}}C + L/R$, $a_2 = k_{\text{pi}}I_L - k_{\text{pi}}I_LD + k_{\text{pi}}U_{\text{o}}/R + k_{\text{ii}}U_{\text{o}}C + (1-D)^2$, $a_3 = k_{\text{ii}}I_L - k_{\text{ii}}I_LD + k_{\text{ii}}U_{\text{o}}/R$, $b_0 = k_{\text{pi}}U_{\text{o}}C$, $b_1 = k_{\text{pi}}I_L - k_{\text{pi}}I_LD + k_{\text{pi}}U_{\text{o}}/R + k_{\text{ii}}U_{\text{o}}C$, $b_2 = k_{\text{ii}}I_L - k_{\text{ii}}I_LD + k_{\text{ii}}U_{\text{o}}/R$.

Then, the closed-loop transfer function of the system can be derived as (25) based on G_{cu}, G_{ui} and G_{i}.

$$G_{\text{u}} = \frac{\hat{u}_{\text{o}}}{\hat{u}_{\text{oref}}} = \frac{G_{\text{cu}}G_{\text{ui}}G_{\text{i}}}{1 + G_{\text{cu}}G_{\text{ui}}G_{\text{i}}} \tag{25}$$

It is obvious that (25) is a high-order transfer function, thus the dual closed-loop needs to be simplified. Considering that the bandwidth of the current loop is wider than that of the voltage loop, the current loop can be regarded as a first-order inertia link, and G_{i} can be simplified as

$$G_{\text{i}}^* = \frac{\hat{i}_L}{\hat{i}_{L\text{ref}}} = \frac{1}{\tau s + 1} \tag{26}$$

where the time constant τ is related to the bandwidth of the current loop.

Then, the closed-loop transfer function can be rewritten as

$$G_{\text{u}}^* = \frac{\hat{u}_{\text{o}}}{\hat{u}_{\text{oref}}} = \frac{G_{\text{cu}}G_{\text{ui}}G_{\text{i}}^*}{1 + G_{\text{cu}}G_{\text{ui}}G_{\text{i}}^*} = \frac{b_0s^2 + b_1s + b_2}{a_0s^3 + a_1s^2 + a_2s + a_3} \tag{27}$$

where $a_0 = U_{\text{o}}C\tau$, $a_1 = U_{\text{o}}C + I_L(1-D)\tau + U_{\text{o}}\tau/R - k_{\text{pu}}I_LL$, $a_2 = I_L - I_LD + U_{\text{o}}/R + k_{\text{pu}}U_{\text{o}} - k_{\text{pu}}U_{\text{o}}D - k_{\text{iu}}I_LL$, $a_3 = k_{\text{iu}}U_{\text{o}}(1-D)$, $b_0 = -k_{\text{pu}}I_LL$, $b_1 = k_{\text{pu}}U_{\text{o}}(1-D) - k_{\text{iu}}I_LL$, $b_2 = k_{\text{iu}}U_{\text{o}}(1-D)$.

The zero-pole plots of (25) and (27) are given under different equilibrium points to verify the validity of the simplification, as shown in Fig.5. The system parameters are listed in Table 1.

TABLE 1. Converter parameters and control parameters.

Parameter	Value
inductance L	3.5 mH
capacitance C	1650 μF
output voltage reference u_{oref}	600 V
proportional coefficient of current loop k_{pi}	0.07
integral coefficient of current loop k_{ii}	233
proportional coefficient of voltage loop k_{pu}	2.633
integral coefficient of voltage loop k_{iu}	1654.4
switching frequency f_{s}	10 kHz
time constant τ	0.0005

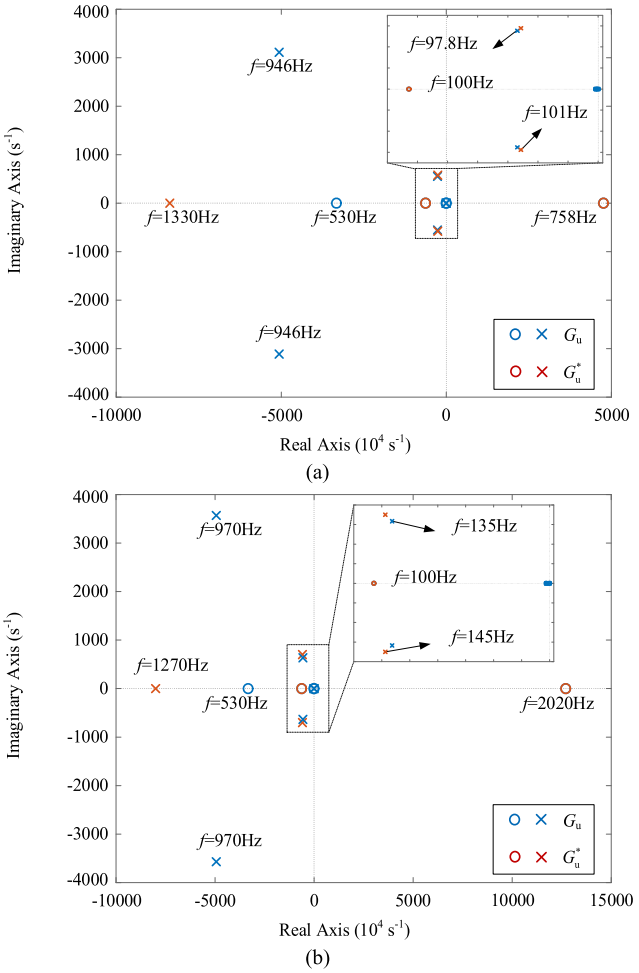

FIGURE 5. Zero-pole plots of (25) and (27). (a) When U_{in} =200 V, I_L =12 A, R = 150 Ω. (b) When U_{in} =400 V, I_L =9 A, R =100 Ω.

It can be found that within the bandwidth of the voltage loop which is about 500 Hz, the conjugate poles of (27) are very close to those of (25), and the remain zeros and poles of the two transfer functions are consistent. It indicates that the characteristics of the two transfer functions are the same at low frequencies, and thus it is valid to analyze the system stability within the control bandwidth based on the simplified transfer function.

Consequently, the Hurwitz criterion of the system can be derived from (27) as

$$\begin{cases} a_0 = U_o C\tau > 0 \\ a_1 = U_o C + I_L(1-D)\tau + U_o\tau/R - k_{pu} I_L L > 0 \\ a_2 = I_L(1-D) + U_o/R + k_{pu}U_o(1-D) - k_{iu} I_L L > 0 \\ a_3 = k_{iu}U_o(1-D) > 0 \\ a_1 a_2 - a_0 a_3 > 0 \end{cases} \tag{28}$$

Taking into account power balance equation, the stability conditions of the system can be derived from (28) as (29), and the stability domain of R is also given. The load limit of R is defined as R_{Hurwitz} and presented as (30).

$$\begin{cases} R > R_1 = \dfrac{k_{pu}U_o L - 2U_{in}\tau}{U_{in}C} \\ R > R_2 = \dfrac{k_{iu}U_o^2 L}{k_{pu}U_{in}^2} \\ R > R_3 = \dfrac{k_{pu}^2 U_{in}^2 U_o L + k_{iu}U_{in}U_o^2 LC + \sqrt{\Delta_R}}{2k_{pu}U_{in}^3 C} \end{cases} \tag{29}$$

$$R_{Hurwitz} = \max\{R_1, R_2, R_3\} \tag{30}$$

where $\Delta_R = U_{in}^2 U_o^2 L[(k_{pu}^2 U_{in} + k_{iu}U_o C)^2 L - 4k_{pu}^2 U_{in} C(k_{iu}U_o L - 2U_{in})]$.

The same process is conducted in CCL case and CPL case. The stability conditions and the stability domain of i_{Load} are derived as (31). The load limit i_{Hurwitz} are presented as (32).

$$\begin{cases} i_{\text{Load}} < i_1 = \dfrac{U_{in}U_o C}{k_{pu}U_o L - U_{in}\tau} \\ i_{\text{Load}} < i_2 = \dfrac{k_{pu}U_{in}^2}{k_{iu}U_o L - U_{in}} \\ i_{\text{Load}} < i_3 = \dfrac{k_{pu}^2 U_{in}^2 U_o L + k_{iu}U_{in}U_o^2 LC - \sqrt{\Delta_i}}{2(k_{pu}k_{iu}U_o^2 L^2 - k_{pu}U_{in}U_o L)} \end{cases} \tag{31}$$

$$i_{\text{Hurwitz}} = \min\{i_1, i_2, i_3\} \tag{32}$$

where $\Delta_i = U_{in}^2 U_o^2 L[(k_{pu}^2 U_{in} + k_{iu}U_o C)^2 L - 4k_{pu}^2 U_{in} C(k_{iu}U_o L - U_{in})]$.

The stability conditions and the stability domain of P_{Load} are derived as (33). The load limit P_{Hurwitz} are presented as (34).

$$\begin{cases} P_{\text{Load}} < P_1 = \dfrac{U_{in}U_o C}{k_{pu}L} \\ P_{\text{Load}} < P_2 = \dfrac{k_{pu}U_{in}^2}{k_{iu}L} \\ P_{\text{Load}} < P_3 = \dfrac{k_{pu}^2 U_{in}^2 L + k_{iu}U_{in}U_o LC - \sqrt{\Delta_P}}{2k_{pu}k_{iu}L^2} \end{cases} \tag{33}$$

$$P_{\text{Hurwitz}} = \min\{P_1, P_2, P_3\} \tag{34}$$

where $\Delta_P = U_{in}^2 L^2[(k_{pu}^2 U_{in} + k_{iu}U_o C)^2 - 4k_{pu}k_{iu}U_{in}U_o C(k_{pu} - k_{iu}\tau)]$.

It is obvious by comparing (13)/(17)/(21) with (29)/(31)/(33) that $R_{\text{MPT}}/i_{\text{MPT}}/P_{\text{MPT}}$ are respectively equivalent to $R_1/i_1/P_1$, when U_{in} is much less than $U_o^2 k_{pu}k_{pi}$ and τ is small enough due to the high switching frequency. Moreover, the relationships between $R_{\text{MPT}}/i_{\text{MPT}}/P_{\text{MPT}}$ and $R_{\text{Hurwitz}}/i_{\text{Hurwitz}}/P_{\text{Hurwitz}}$ which are related to $R_1/i_1/P_1$ need to be discussed.

$R_{\text{MPT}}/i_{\text{MPT}}/P_{\text{MPT}}$ and $R_{\text{Hurwitz}}/i_{\text{Hurwitz}}/P_{\text{Hurwitz}}$ varying with the duty ratio D are obtained based on the parameters in Table 1, and the corresponding stability domains are given, as shown in Fig.6. It can be found that under different system parameters, the stability domains given by the proposed MPT criterion are always larger than those given by the Hurwitz criterion in CIL/CCL/CPL cases.

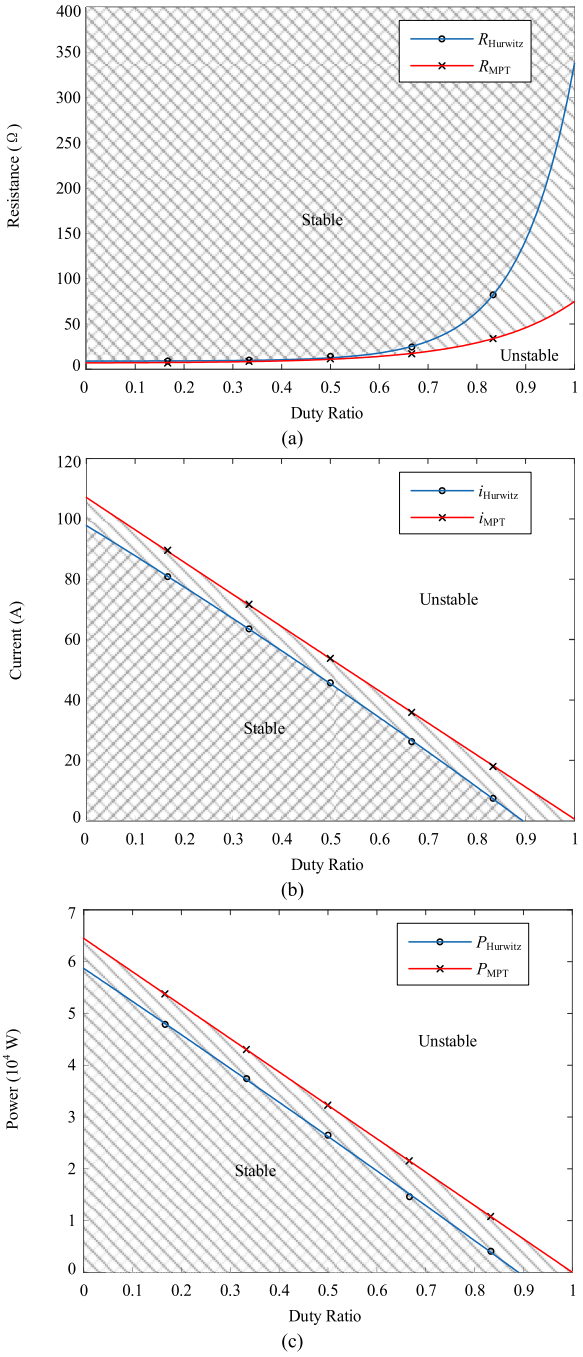

FIGURE 6. Stability domains given by the Hurwitz criterion and the proposed MPT criterion where duty ratio D is the variable. (a) CIL case. (b) CCL case. (c) CPL case.

Therefore, from the aspect of mathematics, the proposed MPT criterion is one of the stability conditions of the Hurwitz criterion and is more optimistic than the Hurwitz criterion, which implies that the proposed MPT criterion is a necessary condition for system stability.

B. PHYSICAL IMPLICATION AND GEOMETRIC INTERPRETATION

The physical implication of the proposed MPT criterion is interpreted by the geometric method in this section to explain the optimism of the criterion and prove the necessity of the criterion for system stability.

According to the control scheme in Fig.1, at the initial control stage, the error between i_{Lref} and i_L is so large that d reaches saturation immediately and switch S keeps turned on in a period of time. Only when i_L becomes larger than i_{Lref}, the PI controller of the current loop performs negative integral, then d decreases and switch S turns off. Therefore, one of the necessary conditions for system stability can be stated that during the first rising period of i_L, if for $t > t_0 > 0$,

$$i_L(t_0) - i_{Lref}(t_0) < 0 \tag{35}$$

and

$$i_L(t) - i_{Lref}(t) \geq \delta, \quad \delta > 0 \tag{36}$$

then the system may work at equilibrium points when $t \to \infty$.

Take the CIL case for example, during the closure of switch S, the differential equations of the system are presented as (37) and solved as (38), where U_{co} represents the initial voltage of the capacitor.

$$\begin{cases} L\dfrac{di_L}{dt} = u_{in} \\ C\dfrac{du_o}{dt} = -\dfrac{u_o}{R} \end{cases} \tag{37}$$

$$\begin{cases} i_L = \dfrac{u_{in}}{L}t \\ u_o = U_{co}e^{-\frac{1}{RC}t} \end{cases} \tag{38}$$

As the output of the PI controller of the voltage loop shown in Fig.1, iL_{ref} is expressed as

$$\begin{aligned} i_{Lref} &= k_{pu}(u_{oref} - u_o) + k_{iu}\int (u_{oref} - u_o)dt \\ &= k_{iu}u_{oref}t + \left(k_{iu}U_{co}RC - k_{pu}U_{co}\right)e^{-\frac{1}{RC}t} \\ &\quad + k_{pu}u_{oref} - k_{iu}U_{co}RC \end{aligned} \tag{39}$$

The surfaces of $i_L(t)$ and $i_{Lref}(t)$ varying with the value of R under different source voltages are drawn based on the parameters in Table 1, as shown in Fig.7.

Then the necessary condition for system stability can be stated by the geometric method that as time t increases, if the surface $i_{Lref}(t)$ can intersect with the surface $i_L(t)$ at a certain time t_0, the system may work at equilibrium points. The minimum load value corresponding to the intersection of the two surfaces is defined as the load limit $R_{Surface}$.

$R_{Surface}$ obtained by the geometric method under different source voltages and R_{MPT} calculated by the proposed MPT criterion are respectively listed in Table 2 for comparison.

In CCL case, $i_L(t)$ and $i_{Lref}(t)$ are derived as

$$\begin{cases} i_L = \dfrac{u_{in}}{L}t \\ i_{Lref} = \dfrac{k_{iu}i_{Load}}{2C}t^2 + (\dfrac{k_{pu}i_{Load}}{C} + k_{iu}u_{oref} - k_{iu}U_{co})t \\ \qquad +k_{pu}(u_{oref} - U_{co}) \end{cases} \tag{40}$$

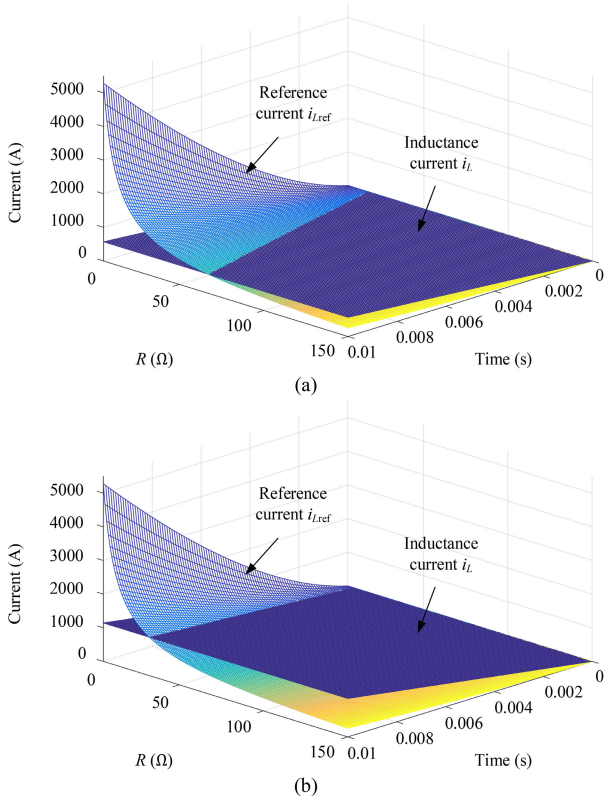

FIGURE 7. Surfaces of $i_L(t)$ and $i_{Lref}(t)$ in CIL case. (a) When $u_{in} = 200$ V. (b) When $u_{in} = 400$ V.

TABLE 2. Load limits of CIL given by geometric method and MPT.

u_{in} (V)	$R_{Surface}$ (Ω)	R_{MPT} (Ω)
100	33	33.46
200	16	16.7
300	11	11.12
400	8	8.33
500	6	6.65

The surfaces varying with the value of i_{Load} under different source voltages are shown in Fig.8. The maximum load value corresponding to the intersection of the surfaces is labeled as $I_{Surface}$. $I_{Surface}$ and I_{MPT} under different source voltages are respectively listed in Table 3.

According to $i_L(t)$ and $i_{Lref}(t)$ derived as (41), the surfaces in CPL case under different source voltages are shown in Fig.9. $P_{Surface}$ and P_{MPT} are respectively listed in Table 4.

$$\begin{cases} i_L = \dfrac{u_{in}}{L}t \\ i_{Lref} = \dfrac{k_{iu}C}{3P_{Load}}\left(U_{co}^2 - \dfrac{2P_{Load}}{C}t\right)^{\frac{3}{2}} + k_{iu}u_{oref}t \\ \quad -k_{pu}\sqrt{U_{co}^2 - \dfrac{2P_{Load}}{C}t} + k_{pu}u_{oref} - \dfrac{k_{iu}U_{co}^3C}{3P_{Load}} \end{cases} \tag{41}$$

It can be found from Table 2 to Table 4 that under different system parameters, $R_{Surface}/i_{Surface}/P_{Surface}$ are always consistent with $R_{MPT}/i_{MPT}/P_{MPT}$. It indicates that the proposed

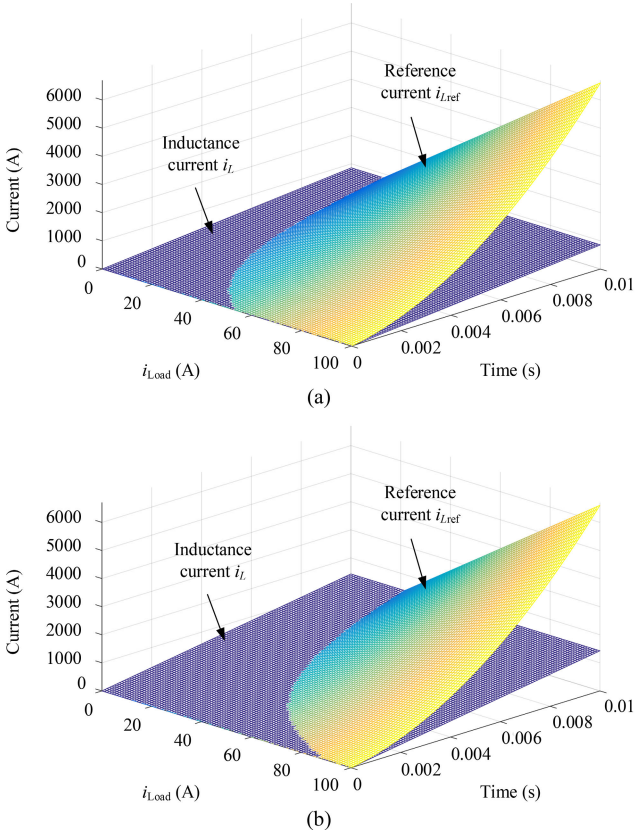

FIGURE 8. Surfaces of $i_L(t)$ and $i_{Lref}(t)$ in CCL case. (a) When $u_{in} = 300$ V. (b) When $u_{in} = 500$ V.

TABLE 3. Load limits of CCL given by geometric method and MPT.

u_{in} (V)	$I_{Surface}$ (A)	I_{MPT} (A)
100	18	17.9
200	36	35.81
300	53	53.71
400	71	71.62
500	90	89.52

MPT criterion only guarantees the normal working of the converter at the initial control stage but not the convergence of the whole control process.

Therefore, the optimism of the proposed MPT criterion is explained from the aspect of control principle that it reflects the working characteristics of the system at the initial control stage and thus provides the necessary condition for system stability. In other words, the stability of the system can be judged from the transient behavior of the converter during the initial control stage, and the system is definitely instable if the system parameters don't satisfy the proposed MPT criterion.

IV. VERIFICATION BASED ON REAL-TIME SIMULATION

The real-time simulation platform used for verification is shown in Fig.10. The system shown in Fig.1 is built in the form of MATLAB/Simulink model in the host computer and then loaded to the real-time simulator RT-LAB (OP 5700) through Ethernet. The simulator is responsible for solving

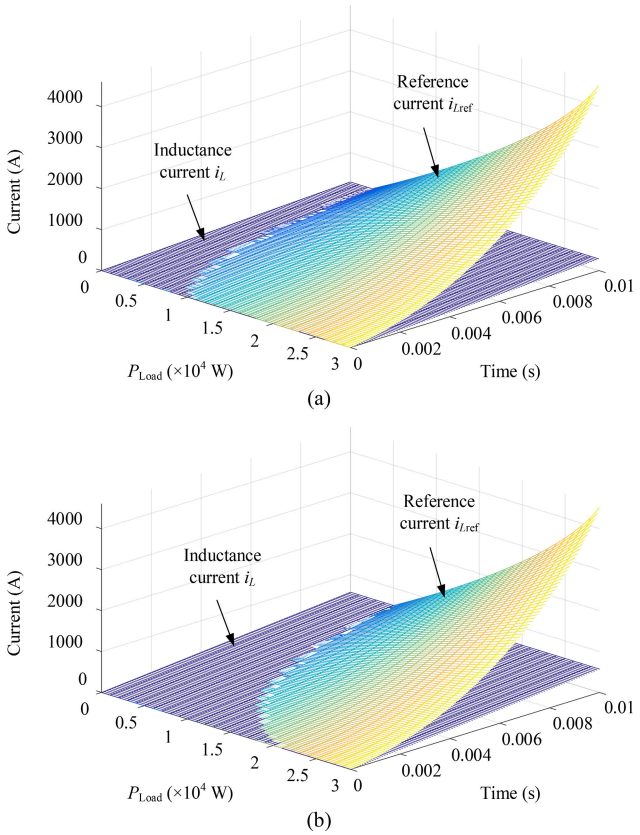

FIGURE 9. Surfaces of i_L(t) and i_{Lref}(t) in CPL case. (a) When u_{in} =100 V. (b) When u_{in} =200 V.

TABLE 4. Load limits of CPL given by geometric method and MPT.

u_{in} (V)	$P_{Surface}$ (W)	P_{MPT} (W)
100	10800	10727
200	21400	21421
300	32000	32083
400	42800	42714
500	53300	53312

the model and generating data. The data is finally transmitted from the simulator to the oscilloscope through I/O interfaces to display the solving results.

The circuit parameters and the control parameters of the system are listed in Table 5. In order to simulate practical working conditions, power-off operation is executed when the system is divergent and the output voltage drops over 5%.

A. VERIFICATION FOR THE PROPOSED CRITERION

The load limits of the system are tested on the platform to verify the proposed criterion. The approach is continuously changing the load value in the stable system, then observing at which value the system starts to be divergent. In different load cases, the final values are defined as the load limits and labeled as $R_{RT-LAB}/I_{RT-LAB}/P_{RT-LAB}$.

Taking the working condition that source voltage u_{in} is set to 300 V for example, the waveforms of output voltage

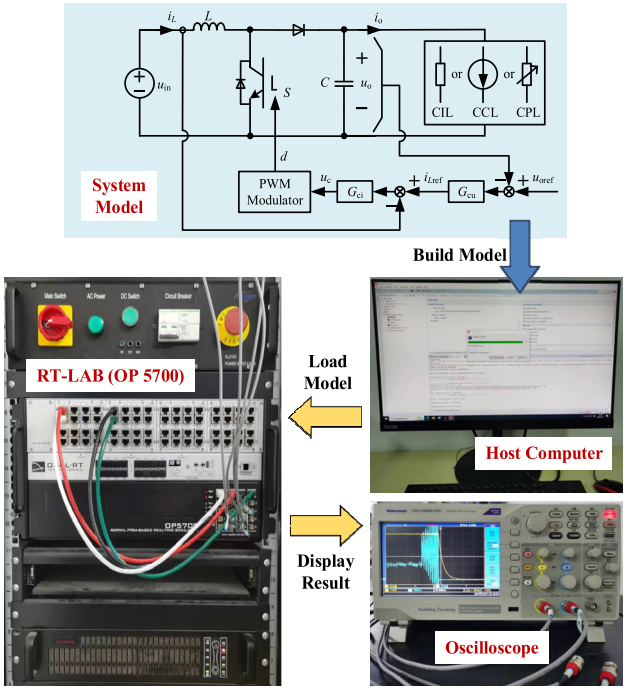

FIGURE 10. Real-time simulation platform.

TABLE 5. System parameters for simulation.

Parameter	Value
inductance L	3.5 mH
capacitance C	1650 μF
output voltage reference u_{oref}	600 V
proportional coefficient of current loop k_{pi}	0.07
integral coefficient of current loop k_{ii}	233
proportional coefficient of voltage loop k_{pu}	2.633
integral coefficient of voltage loop k_{iu}	1654.4
switching frequency f_s	10 kHz

u_o and input current i_L in different load cases are obtained respectively to determine the load limits.

In CIL case, the waveforms of u_o and i_L are shown in Fig.11, where the initial value of R in stable state is 21 Ω and the value is decreased to found the unstable working points. It can be found that u_o drops and i_L increases immediately when the value of R decreases. Both u_o and i_L return to stable state within 4 ms if the value of R is reduced to 15.35 Ω, as shown in Fig.11 (a). While the system becomes divergent and then powered off if the value of R is reduced to 15.34 Ω, as shown in Fig.11 (b). Therefore, R_{RT-LAB} is determined as 15.35 Ω.

After changing the values of i_{Load} in CCL case, the changes of u_o and i_L are shown in Fig.12, where the initial value of i_{Load} is 25 A and then the value is increased to 36 A and 37 A respectively. It is obvious that after the value of i_{Load} is increased to 36 A, the system returns to stable, as shown in Fig.12 (a). But the system becomes divergent and then powered off after the value of i_{Load} changes to 37 A, as shown in Fig.12 (b). Therefore, I_{RT-LAB} is determined as 36 A.

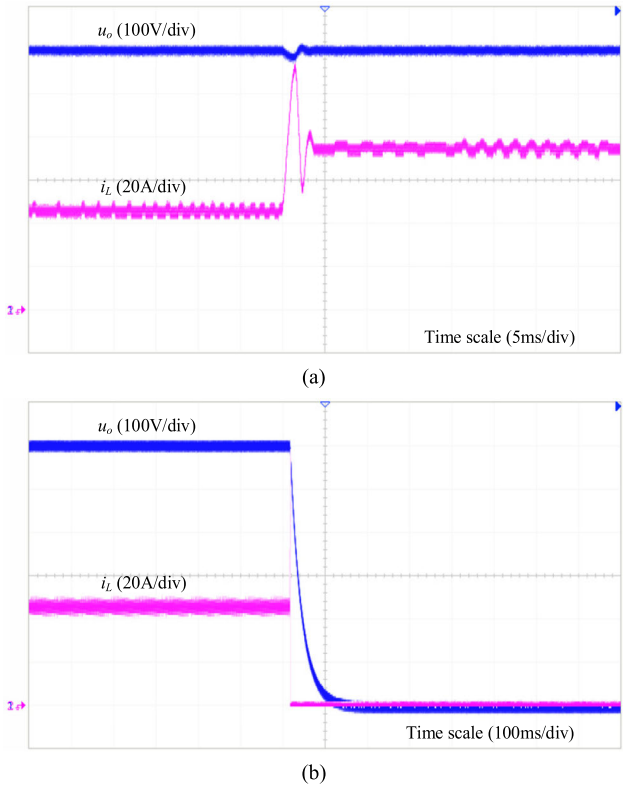

FIGURE 11. Waveforms of u_o and i_L in CIL case. (a) Value of R changes to 15.35 Ω. (b) Value of R changes to 15.34 Ω.

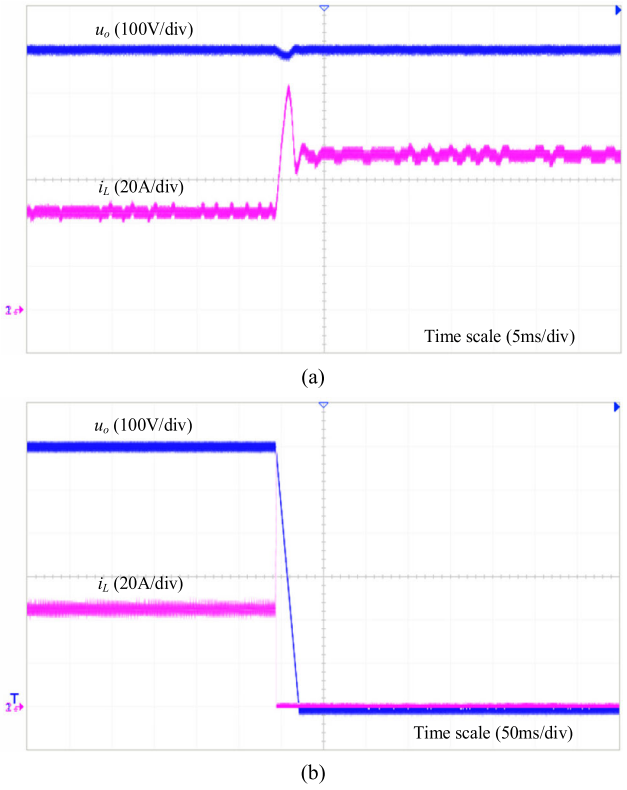

FIGURE 12. Waveforms of u_o and i_L in CCL case. (a) Value of i_{Load} changes to 36 A. (b) Value of i_{Load} changes to 37 A.

The waveforms in CPL case are shown in Fig.13, and the initial value of P_{Load} is 19722 W. The system keeps stable after the value of P_{Load} is increased to 26243 W, while the system becomes unstable after the value of P_{Load} changes to 26244 W, as shown in Fig.13 (a) and Fig.13 (b) respectively. Therefore, $P_{\text{RT-LAB}}$ is determined as 26243 W.

Based on the above method, $R_{\text{RT-LAB}}/I_{\text{RT-LAB}}/P_{\text{RT-LAB}}$ under different source voltages can be tested, and the results are listed in Table 6 to Table 8. Furthermore, the theoretical results calculated by the proposed MPT criterion and the Hurwitz criterion are listed for comparison.

It can be found from Table 6 to Table 8 that under different source voltages, R_{MPT} is always smaller than $R_{\text{RT-LAB}}$, and $I_{\text{MPT}}/P_{\text{MPT}}$ are always larger than $I_{\text{RT-LAB}}/P_{\text{RT-LAB}}$. It denotes that the stability domain obtained from the proposed MPT criterion is larger than the practical stability domain, and thus verifies that the proposed MPT criterion provides the necessary condition for system stability. In addition, compared with $R_{\text{MPT}}/I_{\text{MPT}}/P_{\text{MPT}}$, $R_{\text{Hurwitz}}/I_{\text{Hurwitz}}/P_{\text{Hurwitz}}$ are much closer to $R_{\text{RT-LAB}}/I_{\text{RT-LAB}}/P_{\text{RT-LAB}}$. It indicates that the proposed MPT criterion is more optimistic than the Hurwitz criterion, and the Hurwitz criterion is more accurate for stability analysis. Thus, the conclusions match well with the analyses in Section III and the optimism of the proposed MPT criterion is well verified.

TABLE 6. Theoretical and simulation results for load limit in CIL case.

u_{in} (V)	D	R_{MPT} (Ω)	R_{Hurwitz} (Ω)	$R_{\text{RT-LAB}}$ (Ω)
100	0.833	33.46	82.3	77.44
200	0.667	16.7	24.64	26.22
300	0.5	11.12	14.27	15.35
400	0.333	8.33	10.2	11.43
500	0.167	6.65	7.97	9.68

TABLE 7. Theoretical and simulation results for load limit in CCL case.

u_{in} (V)	D	i_{MPT} (A)	i_{Hurwitz} (A)	$i_{\text{RT-LAB}}$ (A)
100	0.833	17.9	7	7
200	0.667	35.81	26.2	22
300	0.5	53.71	45.36	36
400	0.333	71.62	63.56	50
500	0.167	89.52	80.86	58

TABLE 8. Theoretical and simulation results for load limit in CPL case.

u_{in} (V)	D	P_{MPT} (W)	P_{Hurwitz} (W)	$P_{\text{RT-LAB}}$ (W)
100	0.833	10727	4547	4644
200	0.667	21421	18189	15243
300	0.5	32083	26488	26243
400	0.333	42714	37413	35127
500	0.167	53312	47883	41579

B. CRITERION COMPARISON

In order to verify the effectiveness of the proposed MPT criterion, the MPT criterion based on the modelling method in [31]

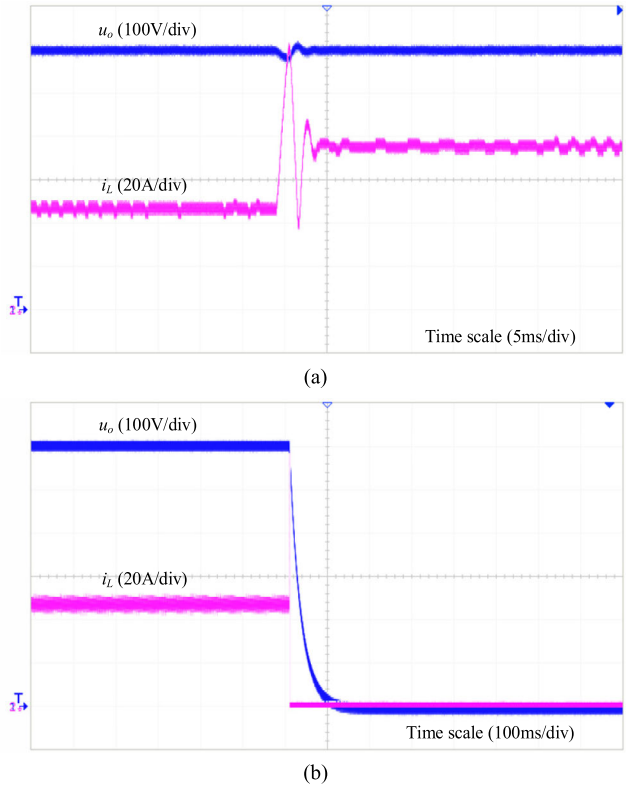

FIGURE 13. Waveforms of u_o and i_L in CPL case. (a) Value of P_{Load} changes to 26243 W. (b) Value of P_{Load} changes to 26244 W.

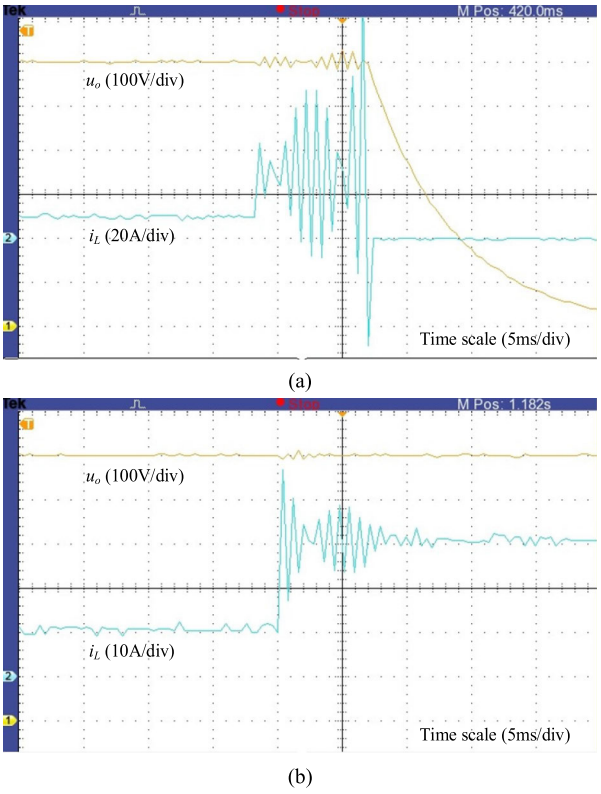

FIGURE 14. Waveforms of u_o and i_L when the value of P_{Load} changes from 3 kW to 9 kW. (a) k_{pu} is set to 7.33. (b) k_{pu} is set to 7.32.

is derived for comparison. The compared MPT criterion in CPL case is presented as

$$\mu_1 + \mu_2 = \frac{1}{C}(k_{pu} - \frac{P_{Load}}{U_o^2} + \frac{1}{R_s}) > 0 \tag{42}$$

where R_s is the equivalent resistance of the current source.

It can be found from (42) that the system stability is only influenced by k_{pu} when C is unchanged, R_s is large enough to be neglected and the system works within the load limit. Therefore, the stability domain of k_{pu} based on the compared MPT criterion can be derived as

$$k_{pu} > \frac{P_{Load}}{U_o^2} - \frac{1}{R_s} \tag{43}$$

According to the expression (19), the stability domain of k_{pu} based on the proposed MPT criterion can be derived as

$$k_{pu} < \frac{U_o U_{in} C}{L P_{Load}} - \frac{U_{in}}{U_o^2 k_{pi}} \tag{44}$$

The stability domain of k_{pu} can be tested based on the same method in the last section. The waveforms of u_o and i_L under the working conditions that P_{Load} changes from 3 kW to 9 kW and 15 kW are shown in Fig.14 and Fig.15 respectively.

As shown in Fig.14, u_o drops and i_L increases immediately when P_{Load} is increased. It is obvious that both of u_o and i_L become divergent if k_{pu} is set to 7.33, as shown in Fig.14 (a). While the system can return to stable state within 10 ms if k_{pu} is set to 7.32, as shown in Fig.14 (b). Therefore, the upper boundary of the stability domain of k_{pu} is determined as 7.32.

Similar phenomenon occurs when P_{Load} changes from 3 kW to 15 kW. The system tends unstable when k_{pu} is set to 4.51 but keeps stable when k_{pu} is set to 4.5, as shown in Fig.15 (a) and Fig.15 (b) respectively. Therefore, the upper boundary of the stability domain of k_{pu} is determined as 4.5.

Based on the above method, the complete stability domain of k_{pu}, including the upper boundary and the lower boundary, is tested under different load changes. The results of (43), (44) and simulation are respectively presented in Table 9.

It can be found from Table 9 that compared to the results of (43), the results of (44) are much closer to the simulation results. The results of (44) fully covers the simulation results, which demonstrates that the proposed MPT criterion is more accurate than the compared MPT criterion. Both of the results of (43) and (44) indicate that when the load changes in a certain range, the system tends unstable as k_{pu} increases, and if k_{pu} is designed improperly, the system may tend divergent as load power increases. It is verified that the influence of system parameters on system stability can be analyzed by the proposed MPT criterion directly which can also be used for the design of system parameters. Thus, the conclusions match well with the analyses in Section II and the effectiveness of the proposed MPT criterion is well verified.

Furthermore, the optimism of the proposed MPT criterion and the compared MPT criterion can also be reflected

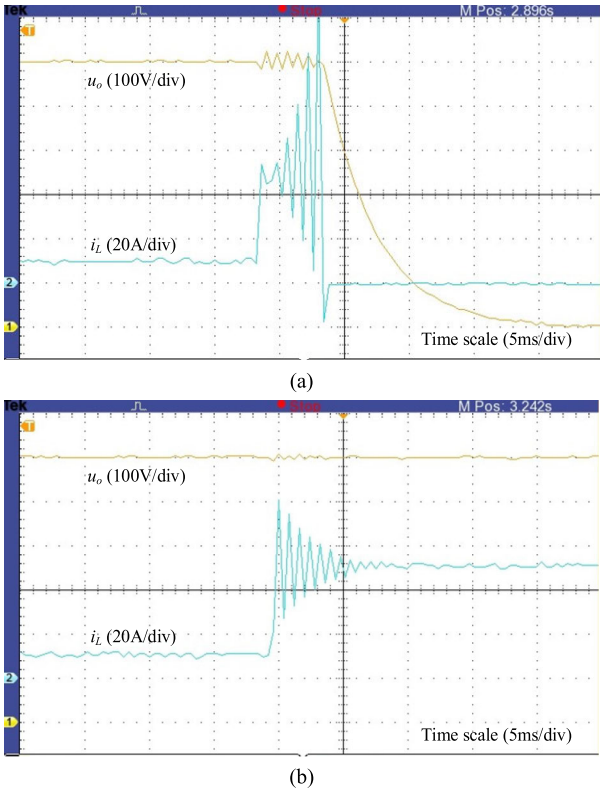

FIGURE 15. Waveforms of u_o and i_L when the value of P_{Load} changes from 3 kW to 15 kW. (a) k_{pu} is set to 4.51. (b) k_{pu} is set to 4.5.

TABLE 9. Theoretical and simulation results for stability domain.

P_{Load} (kW)	Result of (43)	Result of (44)	Simulation
3→6	k_{pu}>0.017	k_{pu}<14.13	0.3<k_{pu}<10.33
3→9	k_{pu}>0.025	k_{pu}<9.42	0.45<k_{pu}<7.32
3→12	k_{pu}>0.033	k_{pu}<7.05	0.6<k_{pu}<5.62
3→15	k_{pu}>0.042	k_{pu}<5.64	0.76<k_{pu}<4.5

from the results in Table 9 but the reasons for the optimism are different. The proposed MPT criterion only involves the transient behavior of the converter during the initial control stage, while the current potential stored by the inductance is neglected in the compared MPT criterion. Although the two stability criteria are incomplete, the parameter ranges can be narrowed by combing the two criteria, and because both criteria are in analytical form, the design of system parameters will be more convenient and accurate.

V. CONCLUSION

In this paper, the stability of a boost-converter system is analyzed based on the MPT method in CIL/CCL/CPL case respectively, and the proposed MPT criterion considers the control parameters of the boost converter. The mathematical features of the proposed MPT criterion are revealed based on the comparison with the Hurwitz criterion, and its physical implication is interpreted by the geometric method. From the aspect of mathematics, the proposed MPT criterion is proved to be one of the stability conditions of the Hurwitz criterion and thus is more optimistic. The reason for the optimism is revealed from the aspect of control principle that the proposed MPT criterion only guarantees the stability of the converter at the initial control stage. Besides, according to the physical implication, the proposed MPT criterion is proved to be the necessary condition for the system stability. The results of the real-time simulations verify the correctness of the theoretical analyses and demonstrate that although the proposed MPT criterion is optimistic, it can still provide instructions for the design of system parameters.

REFERENCES

[1] M. Su, Z. Liu, Y. Sun, H. Han, and X. Hou, "Stability analysis and stabilization methods of DC microgrid with multiple parallel-connected DC–DC converters loaded by CPLs," *IEEE Trans. Smart Grid*, vol. 9, no. 1, pp. 132–142, Jan. 2018, doi: 10.1109/TSG.2016.2546551.

[2] M. Li, Z. Guo, D. Cai, and G. Wang, "Operating characteristic analysis of multi-terminal hybrid HVDC transmission system with different control strategies," in *Proc. Int. Conf. Power Syst. Technol. (POWERCON)*, Guangzhou, China, Nov. 2018, pp. 2616–2621.

[3] M. Vahedipour-Dahraie, A. Anvari-Moghaddam, and J. M. Guerrero, "Evaluation of reliability in risk-constrained scheduling of autonomous microgrids with demand response and renewable resources," *IET Renew. Power Gener.*, vol. 12, no. 6, pp. 657–667, Apr. 2018, doi: 10.1049/iet-rpg.2017.0720.

[4] J. Lu, M. Savaghebi, Y. Guan, J. C. Vasquez, A. M. Y. M. Ghias, and J. M. Guerrero, "A reduced-order enhanced state observer control of DC–DC buck converter," *IEEE Access*, vol. 6, pp. 56184–56191, 2018, doi: 10.1109/ACCESS.2018.2872156.

[5] R. Shah, J. C. Sánchez, R. Preece, and M. Barnes, "Stability and control of mixed AC–DC systems with VSC-HVDC: A review," *IET Gener., Transmiss. Distrib.*, vol. 12, no. 10, pp. 2207–2219, May 2018, doi: 10.1049/iet-gtd.2017.1140.

[6] Y. Li, G. Tang, J. Ge, Z. He, H. Pang, J. Yang, and Y. Wu, "Modeling and damping control of modular multilevel converter based DC grid," *IEEE Trans. Power Syst.*, vol. 33, no. 1, pp. 723–735, Jan. 2018, doi: 10.1109/TPWRS.2017.2691737.

[7] P. Lin, C. Zhang, J. Wang, C. Jin, and P. Wang, "On autonomous large-signal stabilization for islanded multibus DC microgrids: A uniform nonsmooth control scheme," *IEEE Trans. Ind. Electron.*, vol. 67, no. 6, pp. 4600–4612, Jun. 2020, doi: 10.1109/TIE.2019.2931281.

[8] Y. Pan, L. Chen, X. Lu, J. Wang, F. Liu, and S. Mei, "Stability region of droop-controlled distributed generation in autonomous microgrids," *IEEE Trans. Smart Grid*, vol. 10, no. 2, pp. 2288–2300, Mar. 2019, doi: 10.1109/TSG.2018.2849084.

[9] J. Chen and J. Chen, "Stability analysis and parameters optimization of islanded microgrid with both ideal and dynamic constant power loads," *IEEE Trans. Ind. Electron.*, vol. 65, no. 4, pp. 3263–3274, Apr. 2018, doi: 10.1109/TIE.2017.2756588.

[10] Y. Huangfu, S. Pang, B. Nahid-Mobarakeh, L. Guo, A. K. Rathore, and F. Gao, "Stability analysis and active stabilization of on-board DC power converter system with input filter," *IEEE Trans. Ind. Electron.*, vol. 65, no. 1, pp. 790–799, Jan. 2018, doi: 10.1109/TIE.2017.2703663.

[11] L. Meng, Q. Shafiee, G. F. Trecate, H. Karimi, D. Fulwani, X. Lu, and J. M. Guerrero, "Review on control of DC microgrids and multiple microgrid clusters," *IEEE J. Emerg. Sel. Topics Power Electron.*, vol. 5, no. 3, pp. 928–948, Sep. 2017, doi: 10.1109/JESTPE.2017.2690219.

[12] W. Xie, M. Han, W. Cao, J. M. Guerrero, and J. C. Vasquez, "System-level large-signal stability analysis of droop-controlled DC microgrids," *IEEE Trans. Power Electron.*, vol. 36, no. 4, pp. 4224–4236, Apr. 2021, doi: 10.1109/TPEL.2020.3019311.

[13] M. Kabalan, P. Singh, and D. Niebur, "Large signal Lyapunov-based stability studies in microgrids: A review," *IEEE Trans. Smart Grid*, vol. 8, no. 5, pp. 2287–2295, Sep. 2017, doi: 10.1109/TSG.2016.2521652.

[14] D. Marx, P. Magne, B. Nahid-Mobarakeh, S. Pierfederici, and B. Davat, "Large signal stability analysis tools in DC power systems with constant power loads and variable power loads—A review," *IEEE Trans. Power Electron.*, vol. 27, no. 4, pp. 1773–1787, Apr. 2012, doi: 10.1109/TPEL.2011.2170202.

[15] P. Monshizadeh, J. E. Machado, R. Ortega, and A. van der Schaft, "Power-controlled Hamiltonian systems: Application to electrical systems with constant power loads," *Automatica*, vol. 109, Nov. 2019, Art. no. 108527, doi: 10.1016/j.automatica.2019.108527.
[16] W. W. Weaver, R. D. Robinett, D. G. Wilson, and R. C. Matthews, "Metastability of pulse power loads using the Hamiltonian surface shaping method," *IEEE Trans. Energy Convers.*, vol. 32, no. 2, pp. 820–828, Jun. 2017, doi: 10.1109/TEC.2017.2652980.
[17] M. Pavalla, D. Ernst, and D. Ruiz-Vega, *Transient Stability of Power Systems: A Unified Approach to Assessment and Control*. Norwell, MA, USA: Kluwer, 2000, ch. 1, Sec. 5, pp. 17–23.
[18] T. Odun-Ayo and M. L. Crow, "Structure-preserved power system transient stability using stochastic energy functions," *IEEE Trans. Power Syst.*, vol. 27, no. 3, pp. 1450–1458, Aug. 2012, doi: 10.1109/TPWRS.2012.2183396.
[19] S. Pang, S. A. Hashjin, B. Nahid-Mobarakeh, S. Pierfederici, Y. Huangfu, G. Luo, and F. Gao, "Large-signal stabilization of power converters cascaded input filter using adaptive energy shaping control," *IEEE Trans. Transport. Electrific.*, vol. 7, no. 2, pp. 838–853, Jun. 2021, doi: 10.1109/TTE.2020.3021954.
[20] M. A. Hassan, E.-P. Li, X. Li, T. Li, C. Duan, and S. Chi, "Adaptive passivity-based control of DC–DC buck power converter with constant power load in DC microgrid systems," *IEEE J. Emerg. Sel. Topics Power Electron.*, vol. 7, no. 3, pp. 2029–2040, Sep. 2019, doi: 10.1109/JESTPE.2018.2874449.
[21] R. K. Brayton and J. K. Moser, "A theory of nonlinear networks-I," *Quart. Appl. Math.*, vol. 22, no. 1, pp. 1–33, Apr. 1964.
[22] L. Weiss, W. Mathis, and L. Trajkovic, "A generalization of Brayton-Moser's mixed potential function," *IEEE Trans. Circuits Syst. I, Fundam. Theory Appl.*, vol. 45, no. 4, pp. 423–427, Apr. 1998, doi: 10.1109/81.669065.
[23] Z. Li, W. Pei, H. Ye, and L. Kong, "Large signal stability analysis for DC microgrid under droop control based on mixed potential theory," *J. Eng.*, vol. 2019, no. 16, pp. 1189–1193, Mar. 2019, doi: 10.1049/joe.2018.8574.
[24] H. Zheng, L. Zhou, P. Sun, and W. Lu, "Large-signal stability analysis for VSC-HVDC systems based on mixed potential theory," *IEEE Trans. Power Del.*, vol. 35, no. 4, pp. 1939–1948, Aug. 2020, doi: 10.1109/TPWRD.2019.2957270.
[25] B. Li, Y. Liang, G. Wang, H. Li, and X. Chen, "A control parameter design method for hybrid multi-terminal HVDC system," *IEEE Access*, vol. 8, pp. 18669–18680, 2020, doi: 10.1109/ACCESS.2020.2967835.
[26] M. Cucuzzella, K. C. Kosaraju, and J. M. A. Scherpen, "Voltage control of DC microgrids: Robustness for unknown ZIP-loads," *IEEE Control Syst. Lett.*, vol. 7, pp. 139–144, Jul. 2023, doi: 10.1109/LCSYS.2022.3187925.
[27] F. Chang, X. Cui, M. Wang, W. Su, and A. Q. Huang, "Large-signal stability criteria in DC power grids with distributed-controlled converters and constant power loads," *IEEE Trans. Smart Grid*, vol. 11, no. 6, pp. 5273–5287, Nov. 2020, doi: 10.1109/TSG.2020.2998041.
[28] F. Chang, X. Cui, M. Wang, and W. Su, "Region of attraction estimation for DC microgrids with constant power loads using potential theory," *IEEE Trans. Smart Grid*, vol. 12, no. 5, pp. 3793–3808, Sep. 2021, doi: 10.1109/TSG.2021.3081573.
[29] F. Chang, X. Cui, M. Wang, and W. Su, "Potential-based large-signal stability analysis in DC power grids with multiple constant power loads," *IEEE Open Access J. Power Energy*, vol. 9, pp. 16–28, Dec. 2022, doi: 10.1109/OAJPE.2021.3132860.
[30] J. Jiang, F. Liu, S. Pan, X. Zha, W. Liu, C. Chen, and L. Hao, "A conservatism-free large signal stability analysis method for DC microgrid based on mixed potential theory," *IEEE Trans. Power Electron.*, vol. 34, no. 11, pp. 11342–11351, Nov. 2019, doi: 10.1109/TPEL.2019.2897643.
[31] D. Peng, M. Huang, J. Li, J. Sun, X. Zha, and C. Wang, "Large-signal stability criterion for parallel-connected DC–DC converters with current source equivalence," *IEEE Trans. Circuits Syst. II, Exp. Briefs*, vol. 66, no. 12, pp. 2037–2041, Dec. 2019, doi: 10.1109/TCSII.2019.2895842.
[32] G. Zhang, Y. Zheng, Z. Zheng, J. Chen, and T. Hang, "Mixed potential function modeling and stability analysis of DC microgrid with hybrid energy storage," PREPRINT (Version 1), *Tech. Res. Square*, 2024. [Online]. Available: https://www.researchsquare.com/article/rs-2650687/v1, doi: 10.21203/rs.3.rs-2650687/v1.
[33] M. Amin, A. Rygg, and M. Molinas, "Impedance-based and eigenvalue based stability assessment compared in VSC-HVDC system," in *Proc. IEEE Energy Convers. Congr. Expo. (ECCE)*, Milwaukee, WI, USA, Sep. 2016, pp. 1–8.
[34] T. Dragicevic, X. Lu, J. C. Vasquez, and J. M. Guerrero, "DC Microgrids—Part I: A review of control strategies and stabilization techniques," *IEEE Trans. Power Electron.*, vol. 31, no. 7, pp. 4876–4891, Jul. 2016, doi: 10.1109/TPEL.2015.2478859.
[35] M. Amin and M. Molinas, "Small-signal stability assessment of power electronics based power systems: A discussion of impedance- and eigenvalue-based methods," *IEEE Trans. Ind. Appl.*, vol. 53, no. 5, pp. 5014–5030, Sep. 2017, doi: 10.1109/TIA.2017.2712692.
[36] Z.-X. Zou, G. Buticchi, and M. Liserre, "Grid identification and adaptive voltage control in a smart transformer-fed grid," *IEEE Trans. Power Electron.*, vol. 34, no. 3, pp. 2327–2338, Mar. 2019, doi: 10.1109/TPEL.2018.2847020.

YUFEI LI (Graduate Student Member, IEEE) received the B.S. degree in electrical engineering and automation from Shanghai University, Shanghai, China, in 2017, where she is currently pursuing the Ph.D. degree. Her research interests include dc microgrids, dc–dc converters, stability analysis, and control theory.

FEI WANG (Senior Member, IEEE) received the B.S. degree in electrical engineering and the M.S. degree in power electronics from Zhejiang University, Hangzhou, China, in 2002 and 2005, respectively, and the Ph.D. degree in power electronics from Eindhoven University of Technology, Eindhoven, The Netherlands, in 2010.

He was with the Philips Lighting Electronics Global Development Center, Shanghai, China, from 2005 to 2006. He has been a Faculty Member with the School of Mechatronic Engineering and Automation, Shanghai University, Shanghai, since 2010, and became a Professor, in March 2018. He has authored/coauthored more than 100 technical articles, one academic book, and also 13 authorized invention patents. His research interests include distributed generations, electrical drives, power quality, LED drivers, and smart grids.

YUXIN ZHU (Student Member, IEEE) received the M.S. degree in electrical engineering from Shanghai University of Electric Power, Shanghai, China, in 2021. He is currently pursuing the Ph.D. degree with Shanghai University, Shanghai. His research interest includes dc power system stability and control.

HUI GUO (Member, IEEE) received the B.S. degree in electrical engineering from Qingdao University of Science and Technology, Qingdao, China, in 2012, and the Ph.D. degree in electrical engineering from Shanghai University, Shanghai, China, in 2019.

She is currently a Faculty Member with the School of Mechatronic Engineering and Automation, Shanghai University. Her research interests include distributed generations, microgrids, and smart grids.